

# Magnetic domain pinning in an anisotropy-engineered GdTbFe thin film

Stan Konings,<sup>a)</sup> Jorge Miguel, and Jeroen Goedkoop  
*Van der Waals-Zeeman Institute, University of Amsterdam, Valckenierstraat 65, 1018 XE Amsterdam, The Netherlands*

Julio Camarero  
*Departamento de Física de la Materia Condensada, Universidad Autónoma de Madrid, 28049 Madrid, Spain*

Jan Vogel  
*Laboratoire Louis Néel, CNRS, BP 166, F-38042 Grenoble, France*

(Received 17 October 2005; accepted 12 May 2006; published online 7 August 2006)

Focused ion beam irradiation was used to reduce locally the perpendicular anisotropy of magnetic thin films in rectangular lattices of 50 nm sized dots. The effect of the anisotropy patterns, differing in ion fluence and interdot spacing, on the magnetization reversal process was determined in  $q$  space with x-ray resonant magnetic scattering and in real space with magnetic force microscopy. At remanence only a slight alignment of the irregularly shaped domains is observed. In perpendicular magnetic fields, however, the high field bubble domains display a pronounced localization on the dots, showing that this form of local anisotropy reduction is a highly efficient way of domain positioning. © 2006 American Institute of Physics. [DOI: [10.1063/1.2219340](https://doi.org/10.1063/1.2219340)]

## INTRODUCTION

In the past, ion beam irradiation has been used extensively to modify the magnetic anisotropy of thin film materials.<sup>1</sup> Advances in nanotechnology and the data-storage-driven push for control of the magnetic structures on the nanometer scale have revived interest in this technology, where the high-energy ions are used either to cut through the film or to locally change the magnetic anisotropy. In the latter case it is possible to change the pinning landscape without substantially altering the film topology. One approach uses homogeneous ion beams and stencil masks, which allows large areas to be patterned. A more flexible method, restricted to relatively small areas, uses focused ion beam (FIB) patterning to write the desired pattern,<sup>2-6</sup> in which a pencil ion beam is focused to length scales smaller than the domain width.

Most of these studies have centered on FePt and CoPt multilayers with perpendicular magnetic anisotropy (PMA), where the anisotropy reduction is caused by intermixing of the layers.<sup>7-10</sup> Here we present results on PMA rare-earth transition-metal films, a class of materials that is used in magneto-optical recording.<sup>11</sup> The PMA in these materials arises from the surface anisotropy during the growth of the film. By writing rectangular lattices of 50 nm circular dots with various ion fluences, we show that the FIB irradiation locally reduces the PMA on the nanoscale by breaking up the in-grown magnetic pair interactions. We employ the sensitivity and resolution of x-ray resonant magnetic scattering (XRMS) and magnetic force microscopy (MFM) at remanence and in applied field to monitor the evolution of the domain pattern during magnetization reversal. This combination of  $q$ -space and real space techniques gives unique insight into both ensemble-averaged properties such as domain

sizes and distributions and local effects such as domain shape and domain wall pinning. At remanence, the FIB irradiation causes the irregular native domains to have a slight preferential orientation. In perpendicular fields, these domains collapse to bubble domains which are found to localize on the irradiated dots, showing that this is a highly space-efficient and simple way of patterning media. This effect should be present also in other PMA films and could be further optimized using even narrower FIB beams or optimized stencil masks.

## EXPERIMENT

We deposited a 50 nm thin Gd<sub>11.3</sub>Tb<sub>3.7</sub>Fe<sub>85</sub> film using electron beam evaporation at room temperature on a rotating substrate consisting of a silicon nitride coated Si(111) wafer that had a 100 nm thick SiN<sub>x</sub> window at the center. This thin window makes it possible to characterize the film with transmission x-ray resonant magnetic scattering. A 4 nm Al capping layer was deposited on top to protect the film from oxidation. A second film with the same composition and thickness was deposited on a Si(111) wafer and capped with a 2.5 nm Al layer. This film was used for atomic and magnetic force microscopy (AFM/MFM) and hysteresis measurements. Both films were subsequently patterned with a Ga<sup>+</sup> ion beam that was focused to nominally 30 nm, using a beam current of 1 pA and an energy of 30 keV. Nine square lattices of dots were written that varied in interdot spacing  $s$  (nominally 200, 300, and 400 nm) and ion fluence  $f$  ( $1 \times 10^{14}$ ,  $5 \times 10^{14}$ , and  $1 \times 10^{15}$  ions/cm<sup>2</sup> for the sample used for the scattering experiment and  $1 \times 10^{14}$ ,  $1 \times 10^{15}$ , and  $5 \times 10^{15}$  ions/cm<sup>2</sup> for the one used for magnetic force microscopy). The magnetic force microscope is a Digital Instrument Multimode that was used in tapping mode. Large bore coils were placed over the MFM head to generate the perpendicular field during scanning.

<sup>a)</sup>Electronic mail: [konings@science.uva.nl](mailto:konings@science.uva.nl)

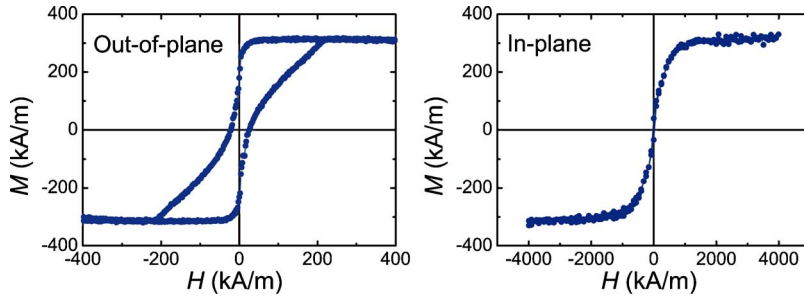


FIG. 1. (Color online) Hysteresis loops of the pristine  $\text{Gd}_{11.3}\text{Tb}_{3.7}\text{Fe}_{85}$  thin film. The out-of-plane loop is measured with polar VSM and the in-plane loop with longitudinal SQUID.

## RESULTS

### Hysteresis

The out-of-plane and in-plane hysteresis loops of the pristine GdTbFe film as measured using polar vibrating-sample magnetometer (VSM) and longitudinal superconducting quantum interference device (SQUID) are shown in Fig. 1. The properties of the film are summarized in Table I. For the in-plane loop, the Stoner-Wohlfahrt model of uniform rotation<sup>11</sup> was used to deduce the uniaxial anisotropy constant  $K_u$  from the saturation magnetization  $M_s$  and the in-plane saturation field  $H_{cr}$  as  $K_u = \frac{1}{2}\mu_0 M_s (H_{cr} - M_s)$ . Using the measured values  $M_s = 320$  kA/m and  $H_{cr} = 1000$  kA/m, we find  $K_u = 1.4 \times 10^5$  J/m<sup>3</sup> and a demagnetization energy constant  $K_d = 6.5 \times 10^4$  J/m<sup>3</sup>. The value for  $K_u$  is close to the one found by Hansen *et al.* ( $1.34 \times 10^5$  J/m<sup>3</sup>).<sup>12</sup> From the composition-dependent exchange stiffness constants of TbFe and GdFe as published by Mimura *et al.*,<sup>13</sup> the exchange stiffness constant  $A$  of our sample is estimated to be about  $1.2 \times 10^{-12}$  J/m. This yields in turn a specific wall energy  $\gamma = 4\sqrt{AK_u}$  of  $1.6 \times 10^{-3}$  J/m<sup>2</sup> and a Bloch wall width  $\delta_b = \pi\sqrt{A/K_u}$  of 9 nm. The characteristic length  $l = \gamma/(2K_d)$  that determines the minimal thickness of the film where equilibrium domain patterns can be formed is 12 nm.

### AFM/MFM

Figure 2 shows the topology of the anisotropy pattern as imaged with AFM. Although the change in topology is small, we can observe the anisotropy dots as small irregular indentations with a diameter of  $\sim 50$  nm and a depth of 2 nm. These values agree well with the predicted sputtering yield of 5.3 atoms/ion as obtained from TRIM (Ref. 14) calculations. From these calculations we also find a  $\text{Ga}^+$  range of 14 nm and an alteration of the amorphous structure over  $\sim 70\%$  of the layer thickness. The indentation depth at high

fluence is still comparable to the 4 nm sample roughness as can be seen from the height profile in Fig. 2. The peaks in the AFM images are probably due to  $\text{Al}_2\text{O}_3$  grains that dominate the sample roughness. This means that anisotropy patterning with FIB at these low fluences is almost nondestructive, leaving the film intact.

The magnetic domain structure of GdTbFe was imaged with MFM both in the remanent state and in *in situ* perpendicular fields. As shown by Fig. 3(b), at remanence, the film exhibits an irregular domain phase with an average domain width of  $\sim 400$  nm. The irregularity originates from thermally activated nucleation<sup>15</sup> and possibly from pinning at local fluctuations in the Tb concentration. The dot pattern is visible on top of the original domain structure as  $\sim 70$  nm diameter areas in which the perpendicular magnetization component is reduced compared to that of the surrounding domain. The dots have smooth edges and there exists a gradual transition to the pristine areas in between dots. The ion implantation is maximum at the center of the dots as the dots render the Gaussian profile of the ion beam. Most probably, the reduction in anisotropy is caused by the collisions during ion implantation which break up the exchange pair interactions that were formed during growth. Remarkably, the writing process does not affect the native domain pattern at remanence, indicating that the gain in domain wall energy is insufficient to overcome the demagnetization forces that

TABLE I. Properties of the pristine  $\text{Gd}_{11.3}\text{Tb}_{3.7}\text{Fe}_{85}$  film.

Film thickness $t$ (nm)	50
Saturation magnetization $M_s$ (A/m)	$3.2 \times 10^5$
In-plane saturation field $H_{cr}$ (A/m)	$1.0 \times 10^6$
Out-of-plane coercivity $H_c$ (A/m)	$1.8 \times 10^4$
Exchange stiffness constant $A$ (J/m)	$1.2 \times 10^{-12}$
Uniaxial energy constant $K_u$ (J/m <sup>3</sup> )	$1.4 \times 10^5$
Demagnetization energy constant $K_d$ (J/m <sup>3</sup> )	$6.5 \times 10^4$
Specific wall energy $\gamma = 4\sqrt{AK_u}$ (J/m <sup>2</sup> )	$1.6 \times 10^{-3}$
Domain wall width $\delta_b = \pi\sqrt{A/K_u}$ (nm)	9
Characteristic length $l = \gamma/(2K_d)$ (nm)	12

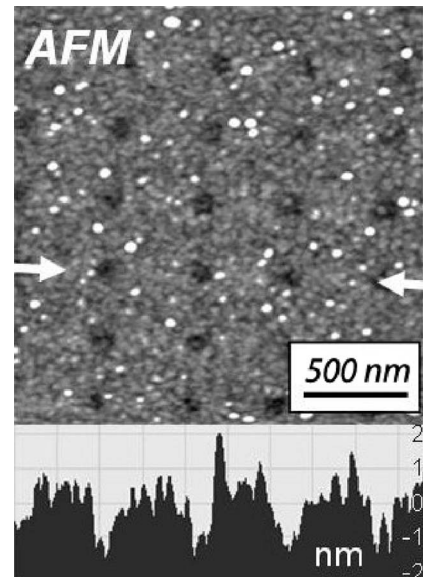


FIG. 2. Atomic force microscopy image of the patterned  $\text{Gd}_{11.3}\text{Tb}_{3.7}\text{Fe}_{85}$  film ( $2 \times 2 \mu\text{m}^2$  scan,  $s = 400$  nm,  $f = 1 \times 10^{15}$  ions/cm<sup>2</sup>). The arrows indicate the position of the height profile as given at the bottom.

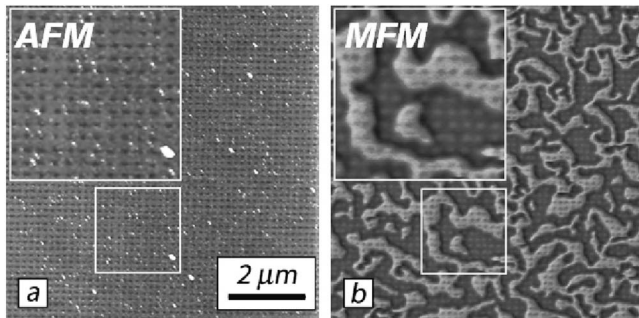


FIG. 3. Atomic force microscopy (a) and corresponding magnetic force microscopy image (b) of an anisotropy dot lattice in  $\text{Gd}_{11.3}\text{Tb}_{3.7}\text{Fe}_{85}$  in the remanent state ( $9 \times 9 \mu\text{m}^2$  scan,  $s=200 \text{ nm}$ ,  $f=1 \times 10^{15} \text{ ions/cm}^2$ ). The insets show the areas indicated by a white box magnified by a factor 2.

produces the original pattern. This is different from our previous study on GdFe in which FIB irradiation was used to align magnetic stripe domains.<sup>6</sup> The stripes in GdFe, which have a well-defined domain width, display an alignment of the Bloch walls on the dots *at remanence* which is clearly not the case here for GdTbFe.

The complete disorder of the domain structure changes in applied magnetic fields. In a 50 kA/m field [Fig. 4(b)], the up domains that have their magnetization aligned to the field grow by domain wall motion until the down domains that are magnetized opposite to the field have a critical width of  $\sim 300 \text{ nm}$ .<sup>16,17</sup> These wormlike down domains have a preference to be positioned on the dots and align to the dot lattice.

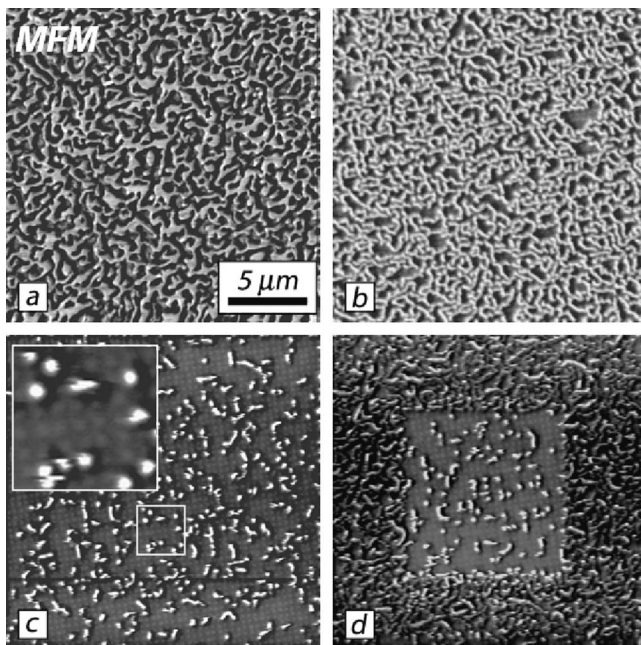


FIG. 4. Magnetic force microscopy images showing the magnetic domain structures of patterned  $\text{Gd}_{11.3}\text{Tb}_{3.7}\text{Fe}_{85}$  in *in situ* perpendicular fields ( $20 \times 20 \mu\text{m}^2$  scan,  $s=400 \text{ nm}$ ,  $f=5 \times 10^{15} \text{ ions/cm}^2$ ). The magnetic domain structure displays an irregular structure at remanence (a), a wormlike structure at 50 kA/m (b), and bubble domains positioned on the dots at 100 kA/m (c) (the inset shows the area in the white box magnified by a factor 3). The considerable tip-induced field can be seen from the  $20 \times 20 \mu\text{m}^2$  scan after measuring several  $10 \times 10 \mu\text{m}^2$  scans at 100 kA/m (d). Down domains that have their magnetization opposite to the field are imaged in light gray.

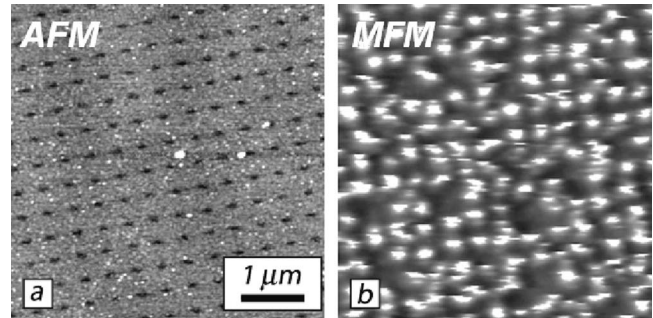


FIG. 5. Atomic force microscopy (a) and corresponding magnetic force microscopy image (b) of an anisotropy dot lattice in  $\text{Gd}_{11.3}\text{Tb}_{3.7}\text{Fe}_{85}$  in an *in situ* perpendicular field of 90 kA/m ( $5 \times 5 \mu\text{m}^2$  scan,  $s=400 \text{ nm}$ ,  $f=5 \times 10^{15} \text{ ions/cm}^2$ ).

When the field is increased to 100 kA/m the wormlike down domains break up in bubble domains that now are positioned on the dots [Figs. 4(c) and 4(d)]. This result is even clearer in Fig. 5 where we compare the topology and magnetic structure of a patterned area at 90 kA/m. Though the tip influence is quite strong at these high fields and clearly visible in these MFM images, the qualitative result is well resolved. The tip-sample interaction can be best observed in Fig. 4(d) where the tip is scanned over the sample at a  $10 \times 10 \mu\text{m}^2$  area. When zoomed out to a scan size of  $20 \times 20 \mu\text{m}^2$ , the different domain structure of the former area is well visible. It takes one extra scan to change the domain structure of the total scan size to the one observed in the  $10 \times 10 \mu\text{m}^2$  scan size. So the magnetic fields reported in the paper are an estimation of the local field induced by the Co-Cr tip that works as a microscopic pole piece. These local fields could be estimated by comparing the magnetization deduced from the MFM images with the hysteresis loop and have to be considered with an error within  $\sim 20\%$ . The external fields generated by the bore coils were roughly three times lower.

## XRMS

Figure 6(a) shows a simplified sketch of the magnetization reversal of a patterned area that emerged from the magnetic force microscopy measurements. The sample shows an

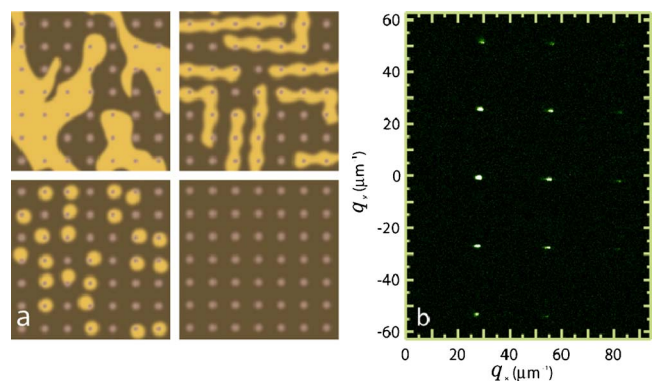


FIG. 6. (Color online) Sketch of the proposed domain structure at different magnetization states (a): at remanence (upper left), at intermediate magnetization (upper right), at high magnetization (lower left), and at saturation field (lower right). (b) shows the measured x-ray resonant magnetic scattering pattern at the Gd  $M_5$  edge of a patterned area at saturation ( $-24 \text{ kA/m}$ ,  $f=1 \times 10^{15} \text{ ions/cm}^2$ ,  $s=225 \text{ nm}$ ).

irregular domain pattern at remanence. At increasingly higher fields, the down domains shrink to form wormlike domains that follow the dot lattice initially and later split up in bubble domains that are pinned on the dots. These bubble domains are ultimately annihilated.

The real space MFM data on the domain structure of the previous section are here combined with data from the  $q$ -space technique x-ray resonant magnetic scattering that provides ensemble-averaged information on magnetic domain sizes and distributions. XRMS is a photon-in photon-out technique, consequently insensitive to applied fields and does therefore not perturb the sample domain structure as compared to MFM.

The x-ray experiments were performed at the soft x-ray beamline ID08 at the European Synchrotron Radiation Facility (ESRF) whose Apple II undulator source offers complete control over the polarization. The sample was illuminated by circularly polarized x rays tuned to the gadolinium  $M_5$  resonance at 1181.5 eV where the substrate window has a transmission of  $\sim 95\%$ . This resonance involves a strong dipole transition between the  $3d$  core level and the unoccupied  $4f$  states, which increases the cross section by orders of magnitude, depending on the angle between the polarization vector and the atomic magnetization direction.<sup>18</sup> Scattering patterns were collected while stepwise increasing the magnetic field from  $-180$  to  $180$  kA/m. The magnetic field was generated by an electromagnet that applied fields perpendicular to the film surface and saturated the sample before the start of the measurement. The experiments were performed with modest photon energy resolution  $\Delta E/E \leq 10^{-3}$  and a beam size of  $100 \mu\text{m}$ . The incident intensity  $I_0$  was monitored by reading the drain current from the refocusing mirror. The resonant scattering signal was collected by a P20 phosphor-coated ( $5 \mu\text{m}$  thick,  $1 \mu\text{m}$  grain size) vacuum window and imaged with a 12 bit charge coupled device camera. A knife edge was used to stop the direct beam.

The MFM results showed us that the reduction of the anisotropy at the dots gives rise to a locally reduced but nonzero magnetization. In the saturated state just before nucleation, this gives rise to a square diffraction pattern with Bragg peaks up to the fifth order as seen in Fig. 6(b). The scattering is relatively weak. For comparison, the color contrast is increased 24 times relative to Fig. 7(b). Such diffraction patterns could be observed in all nine patterned areas, and the intensity of the diffraction spots was found to rise with increasing ion fluence. As expected, the reduction of PMA at the dots depends on ion fluence and is already observed for fluences as low as  $1 \times 10^{14}$  ions/cm<sup>2</sup>. The square diffraction pattern gradually disappears when higher negative fields are applied or when the photon energy is moved away from resonance. Firstly, this confirms that the intensity is indeed resonant magnetic scattering resulting from a modification in the perpendicular magnetization and not from the charge structure due to the implantation of gallium. Secondly, since the area between the dots is saturated perpendicularly to the film, it implies that the atomic moments in the dots have obtained an in-plane anisotropy component. The total integrated intensity of the diffraction pattern increases when approaching remanence. This indicates that the

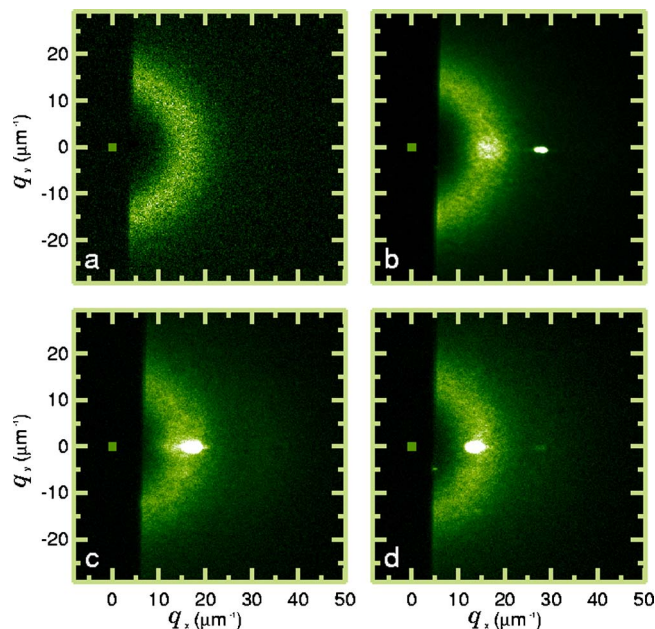


FIG. 7. (Color online) X-ray resonant magnetic scattering patterns at 43 kA/m of a pristine area (a) and the three patterned areas at high ion fluence [ $f=1 \times 10^{15}$  ions/cm<sup>2</sup> and  $s=225$  nm for (b), 340 nm for (c), and 420 nm for (d)]. The origins  $q_r=(0,0)$  are indicated with squares.

moments in the dots rotate from out of plane at high field to in plane at low field where the demagnetizing field dominates.

From the higher order diffraction spots it was possible to determine the interdot spacing with greater accuracy than the nominal values programmed to the FIB system. The interdot spacings were underestimated which was also confirmed by AFM measurements. The accurate values for  $s$  are  $225 \pm 2$ ,  $340 \pm 2$ , and  $420 \pm 2$  nm.

Figure 7 shows the resonant scattering patterns at 43 kA/m of the pristine area and the areas patterned at high fluence. The resonant scattering displays a first order scattering ring which is partly obscured by the beam stop. The intensity in the ring reveals spatial fluctuations which are due to the partial transverse coherence of the  $100 \mu\text{m}$  beam. The scattering ring contains valuable information about the magnetic domain structure. The average domain period can be extracted from the diameter of the ring and the distribution in the domain period can be obtained from its width. The integrated intensity is maximal at zero magnetization and vanishes at magnetic saturation. This behavior is an example of a general rule that relates the reduced magnetization  $m(H)=M(H)/M_{\text{sat}}$  to the scattered intensity as  $I(H) \propto 1 - |m(H)|^2$ .<sup>19</sup> The angular distribution in the scattering ring gives information about the orientations of the domains.

The homogeneous angular distribution in the pristine area demonstrates the totally random orientations of the domains. This homogeneity breaks down when the sample is patterned and clearly a significant increase in scattering in the direction of the dot lattice is observed for all interdot spacings and ion fluences. This reflects the preferential orientation of the irregular domains to the dot lattice while retaining the intrinsic domain period.

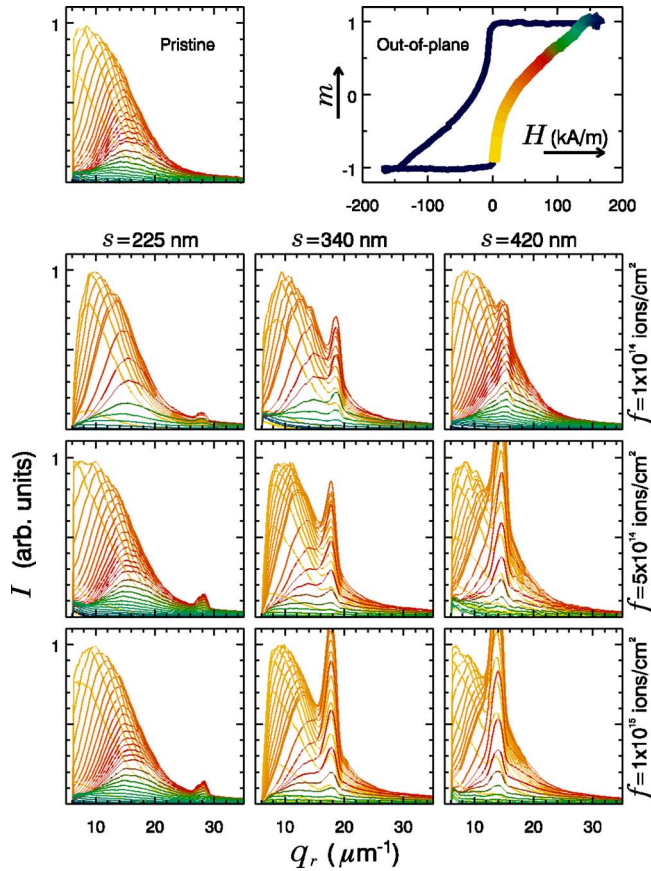


FIG. 8. (Color online) The normalized angularly integrated scattered intensity  $I$  as a function of momentum transfer  $q_r$  of the pristine and nine patterned areas. The color of the line corresponds to the magnetic field as indicated by the out-of-plane hysteresis loop (upper right). The relative magnetization  $m = M/M_{\text{sat}}$  was measured with XMCD.

Also a strong first order diffraction spot is observed at the position that corresponds to the interdot spacing. This diffraction spot can be interpreted as domains that are pinned on the dots and have their domain period adjusted to the interdot spacing. Although the first order diffraction peak can be very strong, second and higher order diffraction peaks are weak which means that there exists no long-range periodicity of the pinned domains. This is displayed in Fig. 6(a) as positional disorder in the wormlike domains and bubbles that are, although pinned, not perfectly aligned on the dots.

The evolution of the angularly integrated scattered intensity as a function of momentum transfer  $q_r$  is displayed in Fig. 8. The magnetic field that corresponds to the individual plots can be extracted from the color coding in the out-of-plane hysteresis loop, measured with x-ray magnetic circular dichroism (XMCD).

For the pristine area, the scattering pattern shows a circularly symmetric intensity disk at the onset of nucleation with no signs of higher orders. As the applied field increases, this disk evolves to a broad ring as observed in Fig. 7(a) which fades out when approaching saturation. The angularly integrated intensity curves of Fig. 8 show a broad peak that reflects the wide distribution of domain periods. The height of the peak quickly rises after nucleation, reaching a maximum at zero magnetization and then gradually decreases, eventually fading out completely at saturation. This quick

rise and gradual fall of the peak height is in agreement with the slope of the hysteresis loop. The peak position, corresponding to the inverse of the domain period, gradually moves to higher momentum transfer  $q$  for higher fields reaching a maximum at 70 kA/m which corresponds to an average domain period of  $\sim 400$  nm. Such behavior is typical for the magnetic reversal via nucleation and domain wall motion as described by Kooy and Enz.<sup>16</sup>

For the patterned areas the first order scattering of the dot lattice stands out as a narrow peak superimposed on the broad peak at the position that we will call  $q_{\text{dot}}$ . The scattered intensities are normalized to the maximum of the broad peak, i.e., the scattered intensity from the unpinned domains. As expected, there exists a wide distribution in the period of the irregular unpinned domains but a much smaller one for the more ordered pinned domains. We also observe a clear trend of growing intensity at  $q_{\text{dot}}$  with higher ion fluence. This demonstrates the higher degree of domain pinning as a consequence of the greater reduction of PMA with higher ion fluence.

In each row of Fig. 8 we observe the rise in domain pinning when going to greater interdot spacings. The intensity at  $q_{\text{dot}}$  rises from a slight contribution at  $s = 225$  nm to the dominant contribution at  $s = 420$  nm. Most probably the intrinsic average domain period ( $\sim 800$  nm) is too large to properly adjust to the smaller interdot spacings.

Though the trend in the ion fluence dependence is quite clear, the presence of stray light contributions in some of the data sets imposed a reduction of the angular integration range. This strongly influences the ratio of the intensities of domain and dot scattering and makes a detailed comparison impossible. For instance, in the case of  $s = 420$  nm,  $f = 5 \times 10^{14}$  ions/cm<sup>2</sup>, the dot scattering is overestimated for this reason.

Although the dependence on ion fluence and interdot spacing can be well extracted from Fig. 8, the evolution of the magnetization reversal can be followed more clearly from Fig. 9. Here the scattered intensity is plotted as a function of field and radial momentum transfer. The position of the maxima of the broad peaks, superimposed on the contour plot, was already discussed for the pristine sample. The magnetization reversals of the patterned areas are remarkably similar, although there are some subtle differences. Especially surprising is the fact that the nucleation and saturation fields are hardly affected by the FIB patterning.

## DISCUSSION

For the MFM and XRMS results of the patterned areas we observe a competition between a magnetization reversal mechanism involving pinned domains and the mechanism as observed in the pristine sample. On the basis of the real space MFM images, the intensity at  $q_{\text{dot}}$  can be interpreted as wormlike domains that follow the dot lattice and split up in bubble domains at higher magnetization as pictured in Fig. 6(a). In this way the periodicity from the dot lattice is imprinted on the pinned domains. Besides we see that the intensity at  $q_{\text{dot}}$  peaks at higher fields compared to the broad peak. This means that most domains are unpinned in the

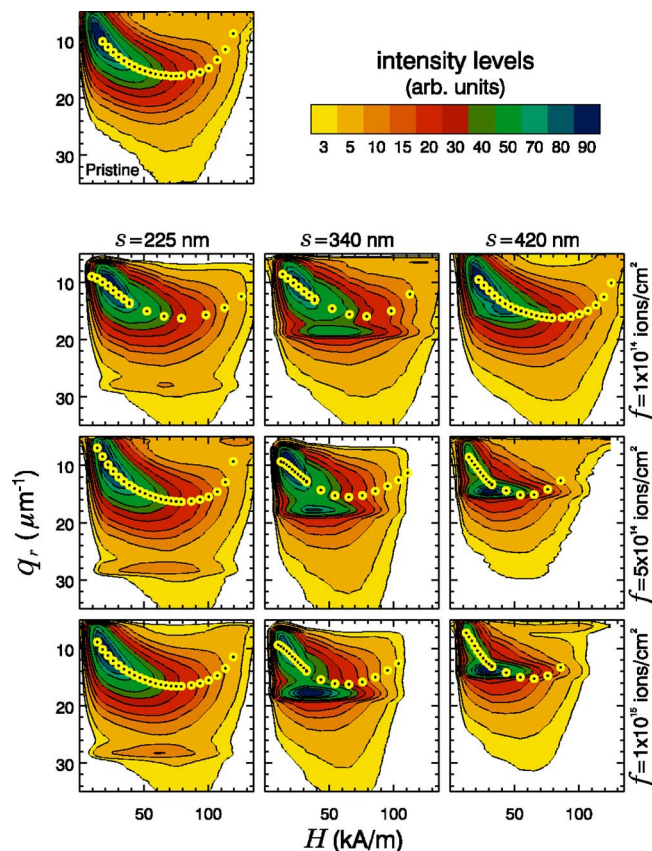


FIG. 9. (Color online) Contour plots of the normalized angularly integrated scattered intensity  $I$  as a function of magnetic field  $H$  and momentum transfer  $q_r$  for the pristine and nine patterned areas. The peak positions of the intensities scattered by the unpinned domains are indicated with circles.

beginning of the magnetization loop but become increasingly pinned when going to higher fields as was observed also in the MFM study. As the decreasing intrinsic domain period approaches the interdot spacing, the pinning on the dot positions becomes more effective.

The reason for this behavior lies in the reduced perpendicular anisotropy in the dots, which results in a local reduction of the out-of-plane magnetization. Consequently, the Zeeman energy, which is the interaction energy of the magnetization with the magnetic field, is reduced in the dots. This effect, also observed in our previous study on GdFe,<sup>6</sup> should be generally present in PMA films and points to a highly efficient way of determining domain positions.

Another very interesting result is that the FIB patterning does not significantly change the apparent nucleation and saturation fields. At first sight this is very surprising, since one expects the lower anisotropy to reduce the nucleation field. It can be understood by noting that in the patterned areas the magnetization rotates more easily with the effective field (applied and demagnetizing) and will partially reverse even before the true nucleation point. The macroscopic nucleation field is, however, the field at which branching into the unpatterned regions in between the dots takes place, and clearly this field is not changed by the patterning. So the reversal of the patterned areas is governed by the barrier for domain wall propagation at the dots and not by domain nucleation as is usually the case.

It is interesting to compare our findings to a study where  $N^+$  ion irradiation was used to mix Co/Pt multilayers<sup>9</sup> in much larger 1400 nm dots. Here the nucleation field was substantially reduced from 360 to 80 kA/m and nucleation occurred primarily at the boundaries of the 1400 nm sized patterns. However, also in this study, the branching of the domains into the unpatterned matrix only started at the as-grown nucleation field. The early nucleation at the boundaries of the patterns is probably triggered by the demagnetizing field of the relatively large patterns, which is absent in the present results as the dots have the same size as a nucleation area [five to eight times the characteristic length (60–96 nm)<sup>20</sup>]. For the same reason, the dots do not affect the macroscopic saturation field appreciably. We can summarize the situation in the statement that the anisotropy dots do not change the nucleation and saturation fields of the matrix in between dots, but they do constitute the *positions* where nucleation and saturation happen.

It has to be pointed out that the effect of the patterning on the domain structure complicates the data analysis of the scattering patterns considerably. In particular, the angular integration of the intensities is not ideal as the scattering from the patterned areas deviates greatly from a ring, especially just after nucleation. Integrating the intensities angularly also eliminates the information about the preferential alignment of the unpinned domains to the dot lattice. This information is, however, conserved in the scattering patterns. A movie in which the scattering patterns of a patterned and a pristine area are compared as a function of field is available online.<sup>21</sup>

## CONCLUSIONS

This paper deals with the effect of lattices of nanosized dots with reduced anisotropy produced with focused ion beam on the magnetization reversal of amorphous GdTbFe thin films. The real space technique of field-dependent magnetic force microscopy that provides local information such as domain shape and domain wall pinning is combined with the  $q$ -space technique of x-ray resonant magnetic scattering that gives insight into the ensemble-averaged magnetic structure in high magnetic fields.

We found that the lowest ion fluence of  $1 \times 10^{14}$  ions/cm<sup>2</sup>, corresponding to only 700 ions per 30 nm diameter dot, is already enough to reduce the perpendicular magnetic anisotropy. The reversal of FIB-patterned areas occurs by two simultaneous competing mechanisms. At low magnetic fields we observe the intrinsic reversal by nucleation and domain wall motion with only a slight preferential domain orientation to the dot lattice. At higher fields, the domains are increasingly pinned on the magnetically soft dots, showing that local irradiation is a very efficient way to localize magnetic domains in very high density lattices. The use of narrower ion beams or stencil masks in combination with more fine grained materials such as FePt multilayers should make further scale reduction of this technique feasible.

## ACKNOWLEDGMENTS

The authors would like to thank H. Luigjes, J. Luigjes, and H. Schlatter from the University of Amsterdam and V. Gadgil of the University of Twente for the preparation of the sample and N. B. Brookes and S. S. Dhesi from the ESRF for their assistance during the measurements. The work is financially supported by the Stichting voor Fundamenteel Onderzoek der Materie (FOM).

- <sup>1</sup>J. C. North, R. Wolfe, and T. J. Nelson, *J. Vac. Sci. Technol.* **15**, 1675 (1978).  
<sup>2</sup>D. McGrouther and J. N. Chapman, *Appl. Phys. Lett.* **87**, 022507 (2005).  
<sup>3</sup>P. Warin, R. Hyndman, J. Gierak, J. N. Chapman, J. Ferre, J. P. Jamet, V. Mathet, and C. Chappert, *J. Appl. Phys.* **90**, 3850 (2001).  
<sup>4</sup>J. Gierak *et al.*, *Appl. Phys. A: Mater. Sci. Process.* **80**, 187 (2005).  
<sup>5</sup>M. Albrecht, C. T. Rettner, M. E. Best, and B. D. Terris, *Appl. Phys. Lett.* **83**, 4363 (2003).  
<sup>6</sup>S. Konings, J. Miguel, J. Luigjes, H. Schlatter, H. Luigjes, and J. Goedkoop, *J. Appl. Phys.* **98**, 054306 (2005).  
<sup>7</sup>C. Chappert *et al.*, *Science* **280**, 1919 (1998).

- <sup>8</sup>J. Fassbender, D. Ravelosona, and Y. Samson, *J. Phys. D* **37**, R179 (2004), and references therein.  
<sup>9</sup>G. J. Kusinski, K. M. Krishnan, G. Denbeaux, G. Thomas, B. D. Terris, and D. Weller, *Appl. Phys. Lett.* **79**, 2211 (2001).  
<sup>10</sup>D. Ravelosona, C. Chappert, V. Mathet, and H. Bernas, *Appl. Phys. Lett.* **76**, 236 (2000).  
<sup>11</sup>M. Mansuripur, *The Physical Principles of Magneto-Optical Recording* (Cambridge University Press, Cambridge, 1995).  
<sup>12</sup>P. Hansen, C. Clausen, G. Much, M. Rosenkranz, and K. Witter, *J. Appl. Phys.* **66**, 756 (1989).  
<sup>13</sup>Y. Mimura, N. Imamura, T. Kobayashi, A. Okada, and Y. Kushiuro, *J. Appl. Phys.* **49**, 1208 (1978).  
<sup>14</sup>J. F. Ziegler and J. P. Biersack, <http://www.srim.org>  
<sup>15</sup>M. Labrune, S. Andrieu, F. Rio, and P. Bernstein, *J. Magn. Magn. Mater.* **80**, 211 (1989).  
<sup>16</sup>C. Kooy and U. Enz, *Philips Res. Rep.* **15**, 7 (1960).  
<sup>17</sup>E. A. Jagla, *Phys. Rev. E* **70**, 046204 (2004).  
<sup>18</sup>J. F. Peters, J. Miguel, M. A. de Vries, O. M. Toulemonde, J. B. Goedkoop, S. S. Dhesi, and N. B. Brookes, *Phys. Rev. B* **70**, 224417 (2004).  
<sup>19</sup>J. Miguel, J. B. Goedkoop, J. Camarero, M. Bonfim, J. Vogel, and N. B. Brookes, *Phys. Rev. B* (submitted).  
<sup>20</sup>T. H. O'Dell, *Rep. Prog. Phys.* **49**, 589 (1986).  
<sup>21</sup>S. Konings, <http://www.science.uva.nl/~konings/fib.html>